

Supplement of Atmos. Chem. Phys., 20, 8511–8532, 2020
<https://doi.org/10.5194/acp-20-8511-2020-supplement>
© Author(s) 2020. This work is distributed under
the Creative Commons Attribution 4.0 License.



Supplement of

Biomass-burning-derived particles from a wide variety of fuels – Part 2: Effects of photochemical aging on particle optical and chemical properties

Christopher D. Cappa et al.

Correspondence to: Christopher D. Cappa (cdcappa@ucdavis.edu)

The copyright of individual parts of the supplement might differ from the CC BY 4.0 License.

1 Model parameter cross-sensitivities and uncertainties

The SOA yields are most sensitive to the initial [NMOG]/[OA] ratio. When the [NMOG]/[OA] ratio is assumed larger, the necessary SOA yields are smaller. There is an approximately inverse relationship between the assumed initial [NMOG] and the SOA yield for each NMOG type (fast, 5 slow, very slow). However, the influence of multi-generational impacts the relationship to some extent.

The O:C ratios for the different SOA types are weakly dependent on the relative abundances specified for the different types. There is also a weak cross-sensitivity between the O:C values specified for the different SOA types, especially between the fast and slow-forming SOA. In 10 general, if the $O:C_{fast}$ is increased, the $O:C_{slow}$ must be decreased. However, only relatively minor variations in the O:C of each type is allowable to obtain reasonable model-measurement agreement, especially at short photochemical ages. The f_{60} values for the different SOA types exhibit similar cross-sensitivities as the O:C values. However, they are generally less sensitive, in comparison, because the f_{60} values are so similar for all SOA types.

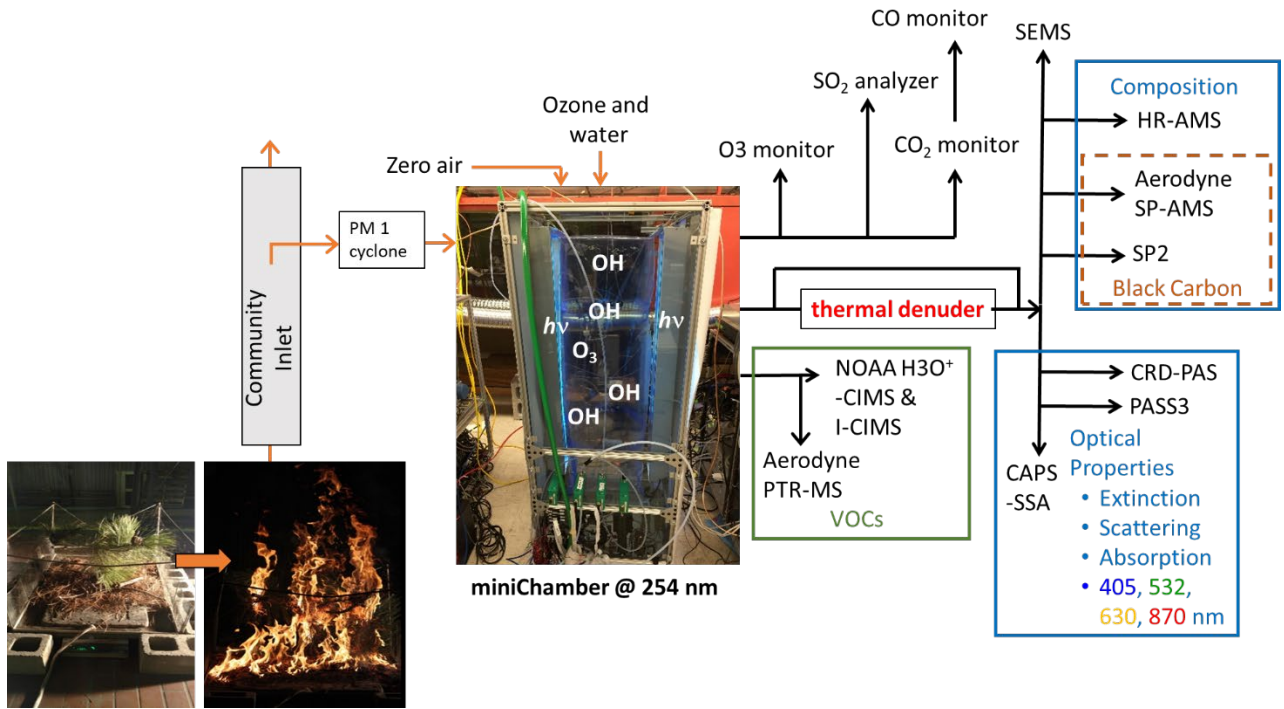
15 The model k_{OH} values also exhibit some dependence on the assumed initial [NMOG]/[OA] and yields. In general, if $k_{OH,fast}$ is decreased the $k_{OH,slow}$ must be increased. However, the $k_{OH,fast}$ is reasonably well-constrained by the rapid rise in the [OA]/[rBC] and O:C for all particle classes, and by the increase in the $MAC_{BrC,405nm}$ that is observed at very short photochemical ages for some of the particle classes. The assumed k_{OH} for multi-generational aging is most sensitive to the choice 20 of the $k_{OH,slow}$, with the two generally exhibiting an inverse relationship.

It is difficult to estimate a comprehensive uncertainty on these values; we qualitatively estimate uncertainties based on the model sensitivity to changing these parameter values. If the MAC_{fast} were as small as the values for the other SOA types the modeled MAC_{BrC} would decline much too rapidly compared to the observations. Also, it is necessary that the MAC_{fast} be greater than the 25 MAC_{BrC} of the primary OA for SSA class 5 and class 6 to reproduce the initial increase at short aging times. However, if the MAC_{fast} were much larger than our estimate the model predicts an initial increase in the MAC_{BrC} for the intermediate SSA classes 3 and 4, in contrast to the observations. We therefore estimate a uncertainty of $\pm 0.2 \text{ m}^2 \text{ g}^{-1}$ based on the model sensitivity to variations in this parameter. The MAC_{slow} values are largely determined by the behavior at 30 intermediate equivalent ages, as this is where they have the largest fractional contributions; we

estimate the uncertainty as $\pm 0.05 \text{ m}^2 \text{ g}^{-1}$. The MAC_{vs} is not especially well-constrained as it only makes up a very small fraction of the OA mass. A value of $MAC_{\text{vs}} = 0.05 \text{ m}^2 \text{ s}^{-1}$ is used for consistency with the MAC_{slow} , but a value of $MAC_{\text{vs}} = 0 \text{ m}^2 \text{ g}^{-1}$, i.e. non-absorbing, is not entirely unreasonable. The $MAC_{2\text{G}}$ and MAC_{het} values are primarily determined by the behavior at long equivalent ages. The estimated uncertainty in $MAC_{2\text{G}}$ is $\pm 0.05 \text{ m}^2 \text{ g}^{-1}$ while the estimated uncertainty in MAC_{het} is $\pm 0.025 \text{ m}^2 \text{ g}^{-1}$. That the MAC_{het} is smaller than the MAC_{BrC} values for the various SOA types indicates that over longer time the overall MAC_{BrC} will continue to decline until it reaches $0.05 \text{ m}^2 \text{ g}^{-1}$.

40

2 Supplemental Figures



45 **Figure S1.** Cartoon schematic of sampling into and from the mini chamber during FIREX. Instrument names are given in

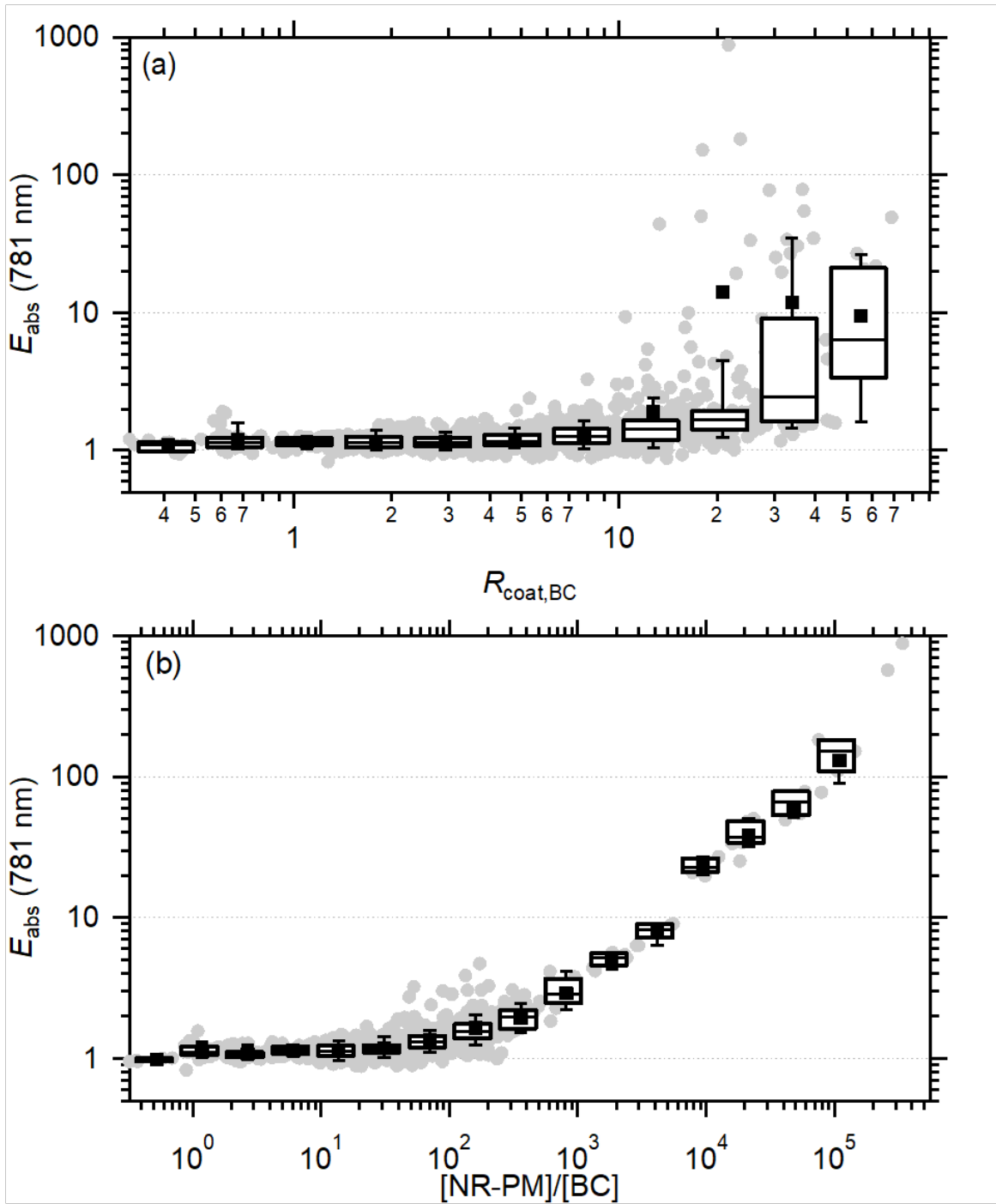


Figure S2. (a) Dependence of the observed E_{abs} 781 nm on the coating-to-rBC core mass ratio, $R_{\text{coat-rBC}}$. (b) Dependence of the E_{abs} at 781 nm on the $[\text{NR-PM}]/[\text{rBC}]$ ratio. The observations have been binned according to either the $R_{\text{coat-rBC}}$ or $[\text{NR-PM}]/[\text{rBC}]$ ratio, shown as box-and-whisker plots.

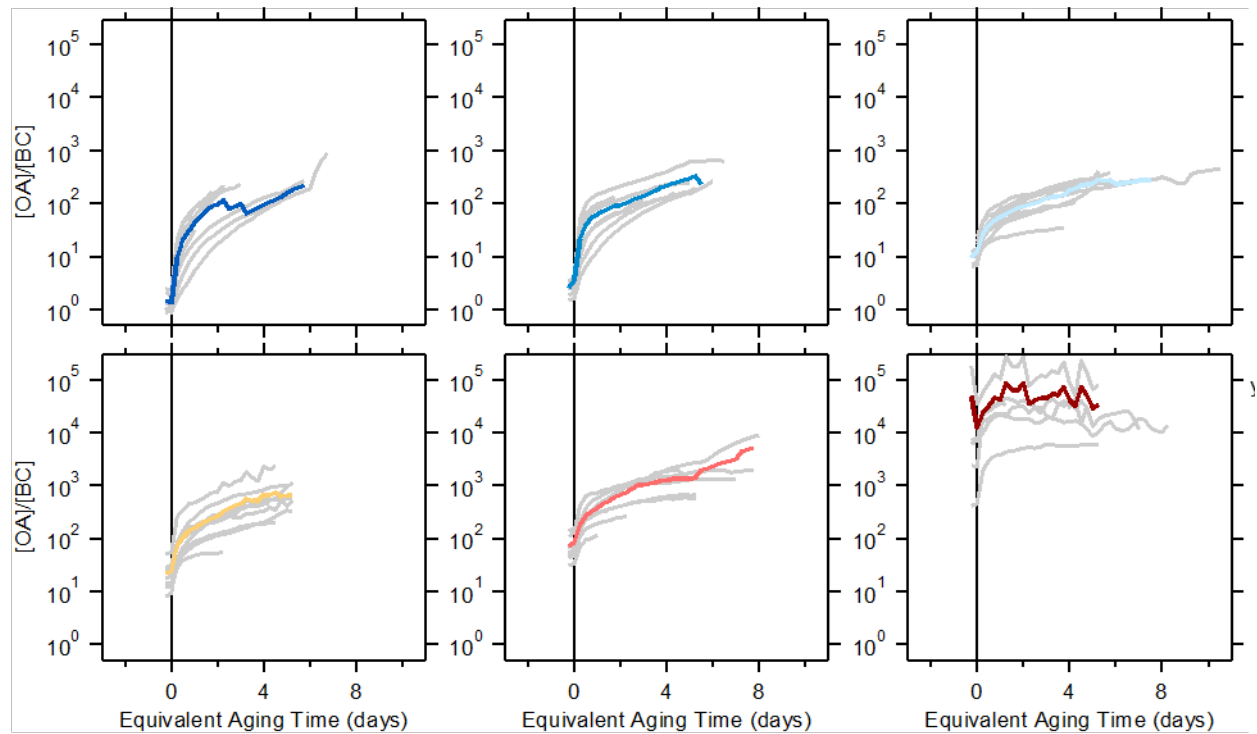


Figure S3. Relationship between $[OA]/[BC]$ and the equivalent atmospheric aging time for each SSA classification. Individual burns are shown as gray lines, and the average for each SSA class as the colored line.

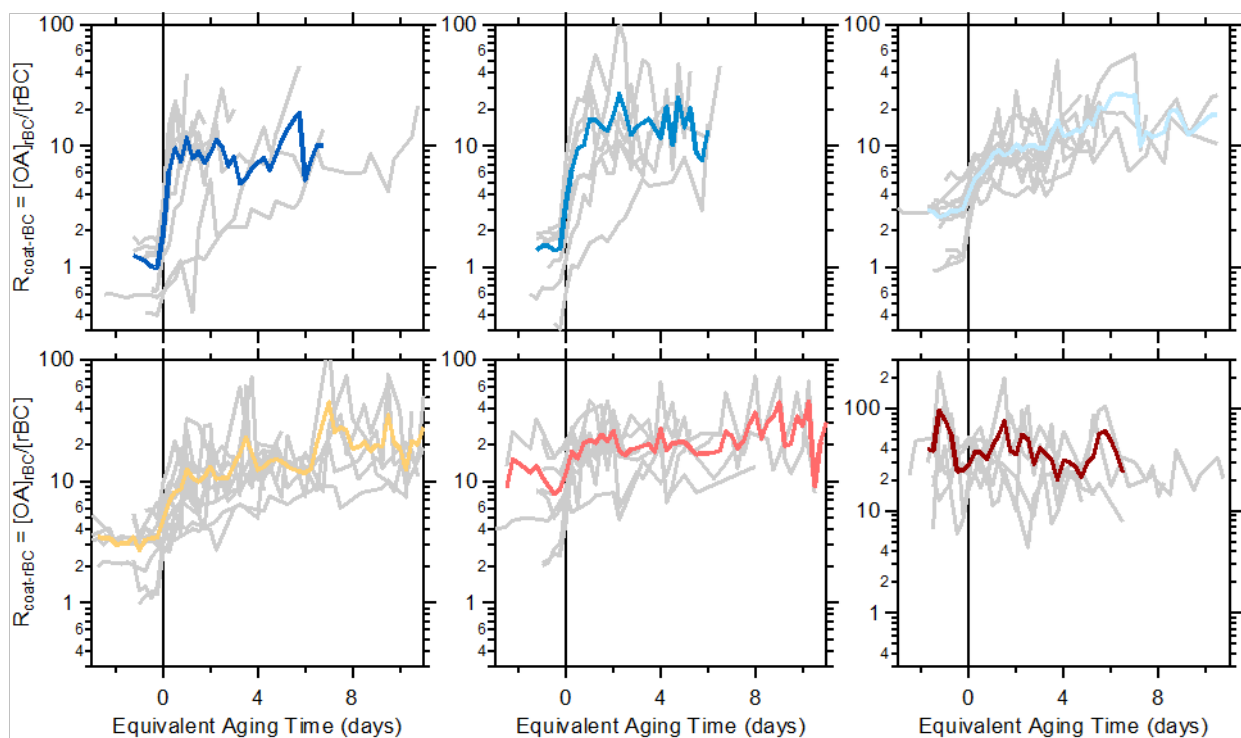
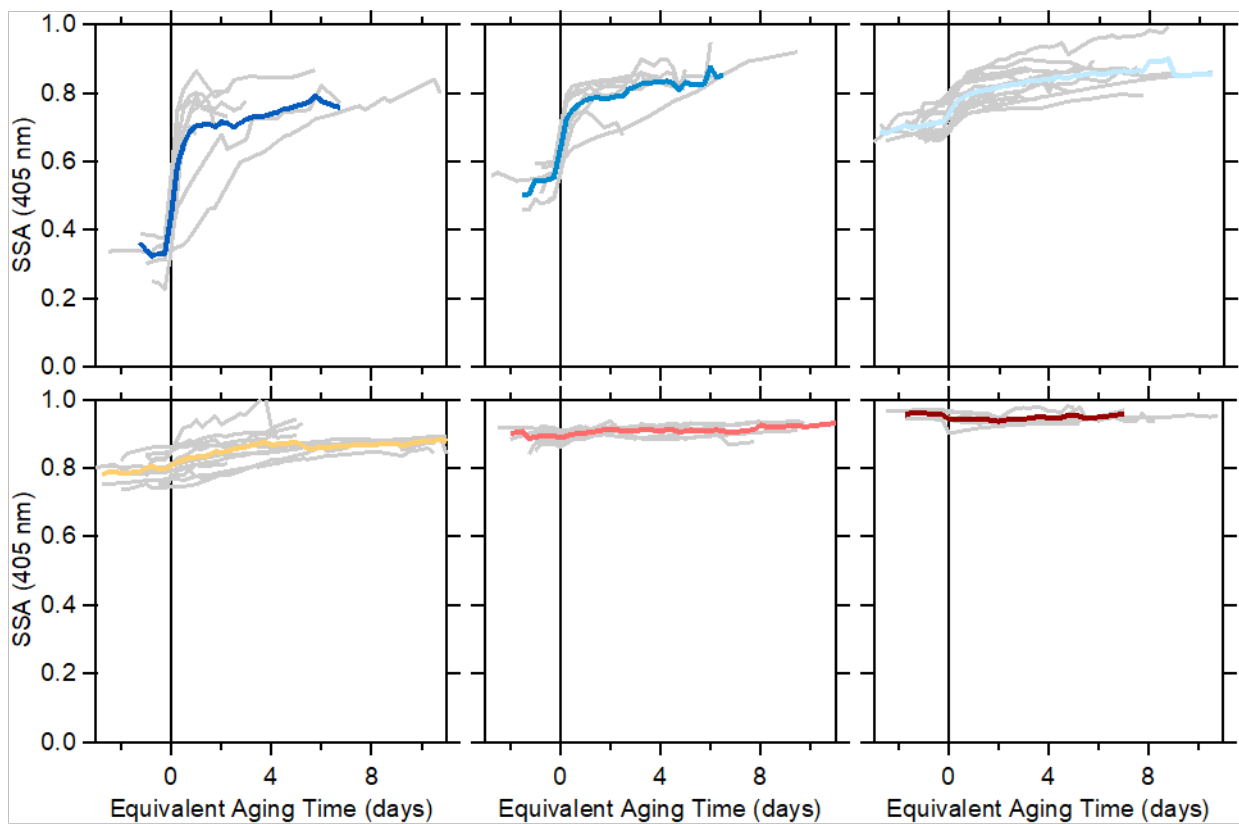
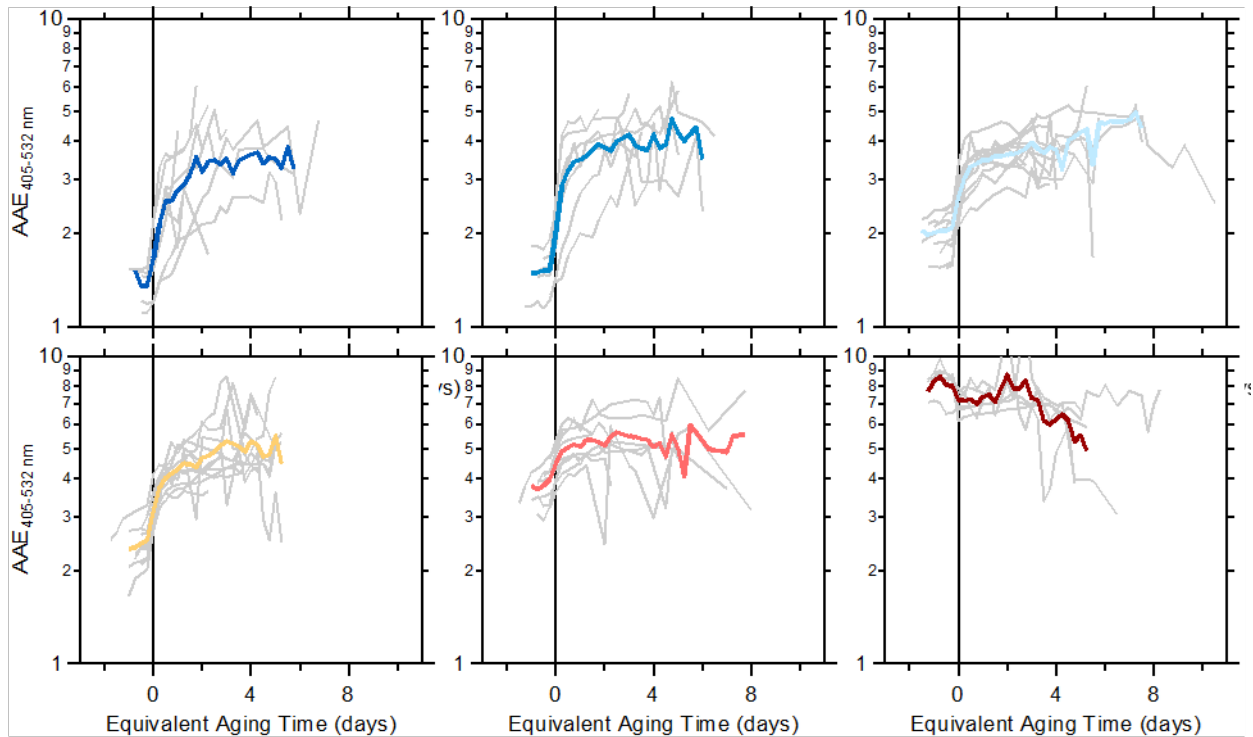


Figure S4. Relationship between $R_{\text{coat-rBC}}$ and the equivalent atmospheric aging time for each SSA classification. Individual burns are shown as gray lines, and the average for each SSA class as the colored line.

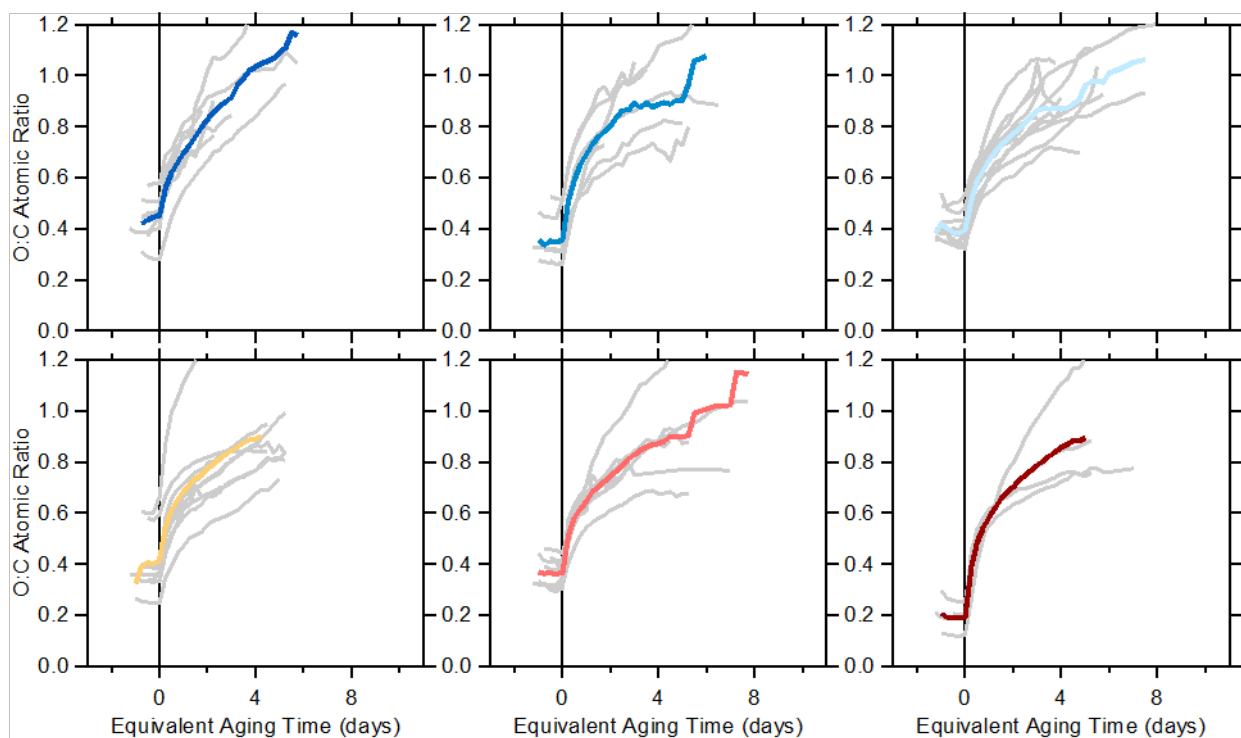
65



70 **Figure S5.** Relationship between SSA at 405 nm and the equivalent atmospheric aging time for each SSA classification. Individual burns are shown as gray lines, and the average for each SSA class as the colored line.



75 **Figure S6.** Relationship between the AAE₄₀₅₋₅₃₂ and the equivalent atmospheric aging time for each SSA classification. Individual burns are shown as gray lines, and the average for each SSA class as the colored line.



80

Figure S7. Relationship between the O:C atomic ratio at 405 nm and the equivalent atmospheric aging time for each SSA classification. Individual burns are shown as gray lines, and the average for each SSA class as the colored line.

85

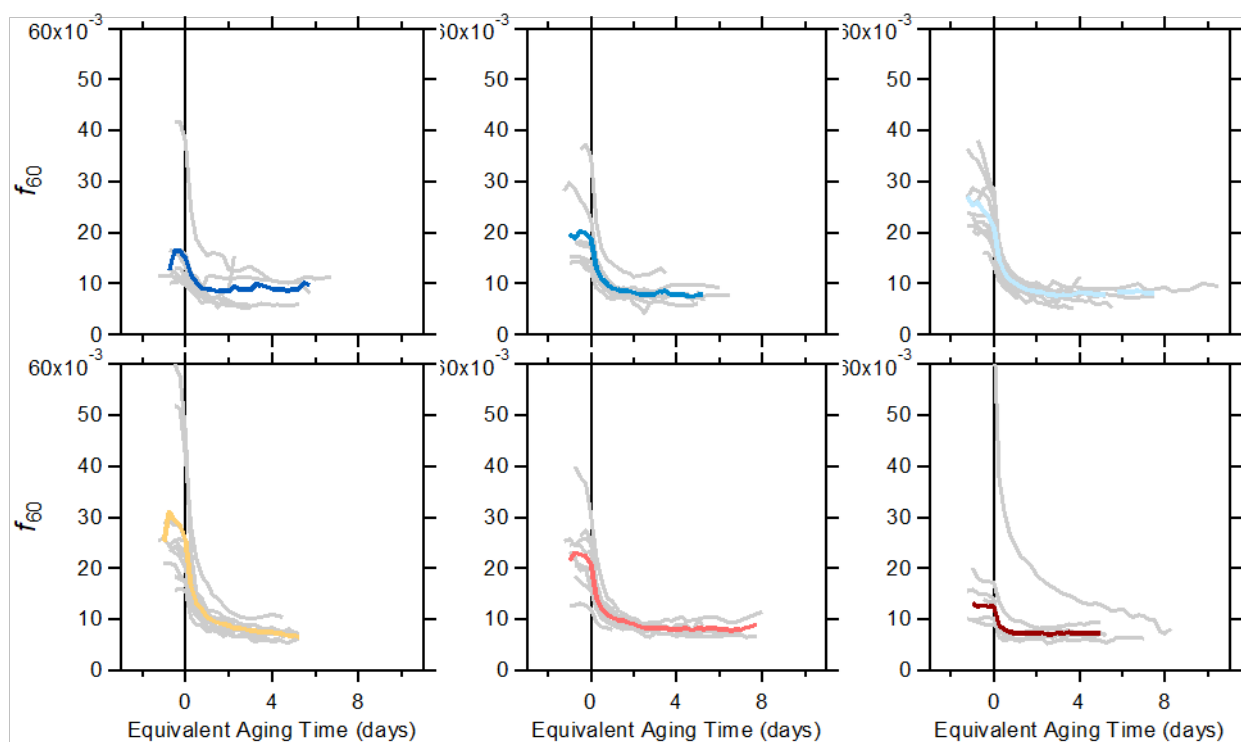
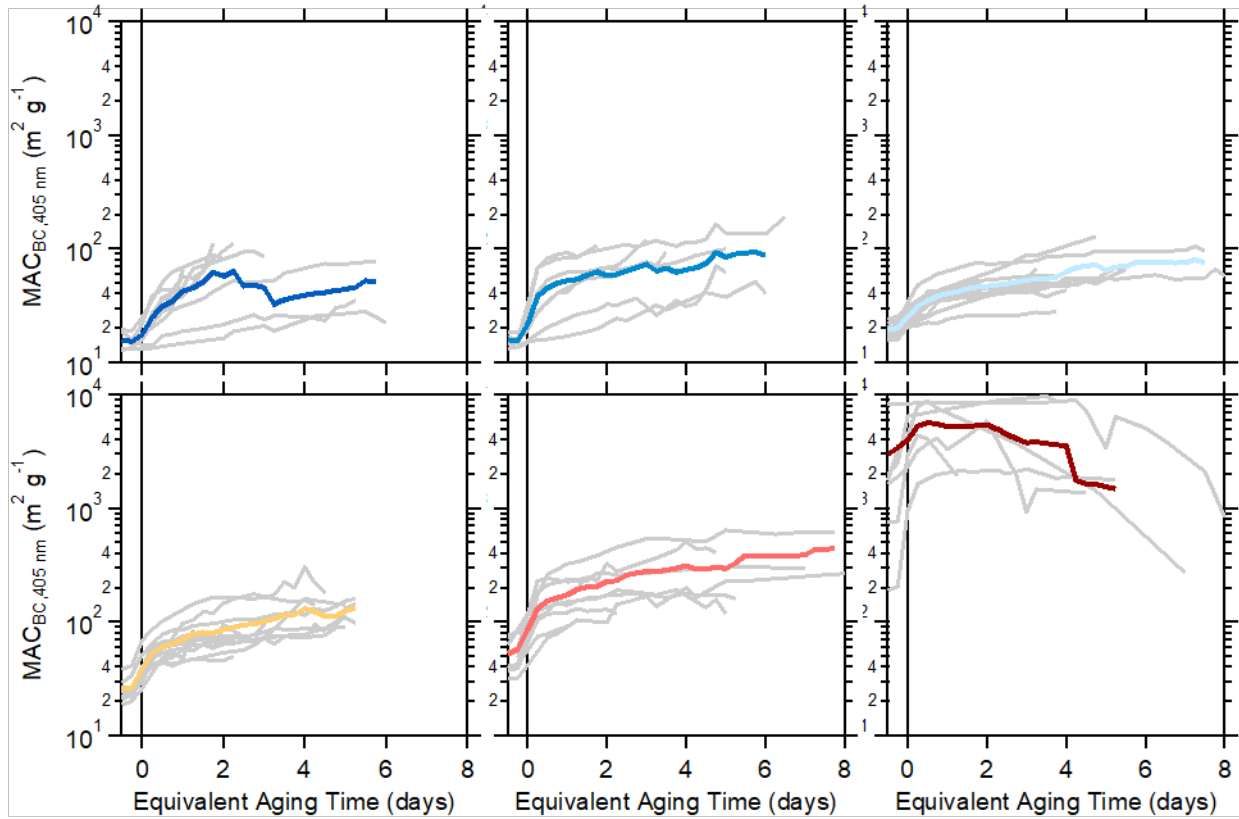
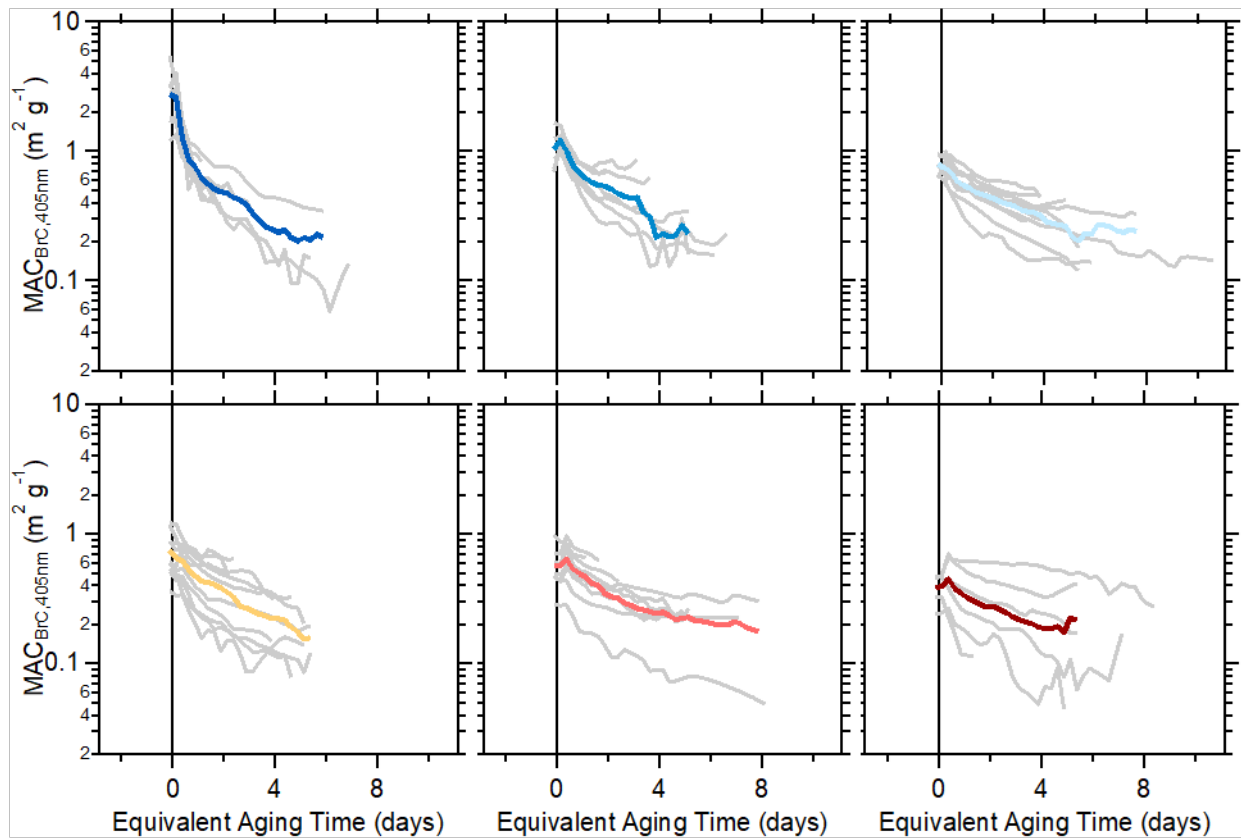


Figure S8. Relationship between the AMS f_{60} and the equivalent atmospheric aging time for each SSA classification. Individual burns are shown as gray lines, and the average for each SSA class as the colored line.

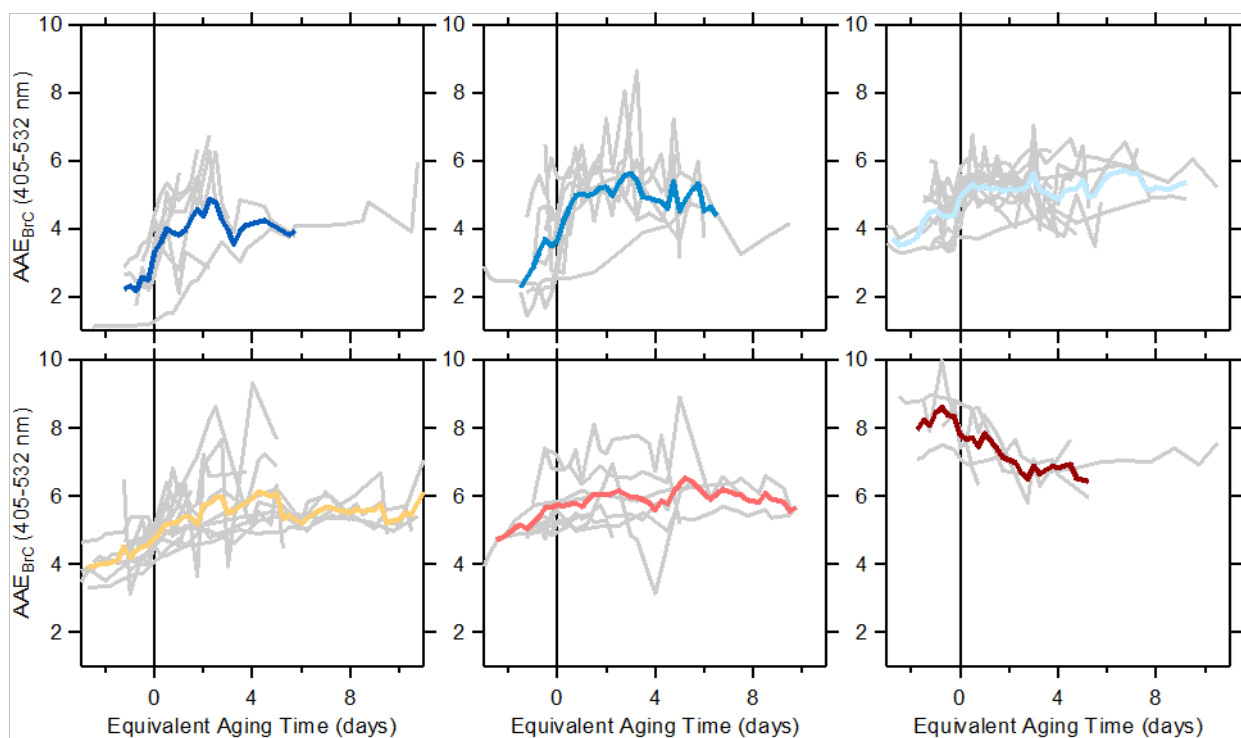
90



95 **Figure S9.** Relationship between the $MAC_{BC,405\text{ nm}}$ and the equivalent atmospheric aging time for each SSA classification. Individual burns are shown as gray lines, and the average for each SSA class as the colored line.



100 **Figure S10.** Relationship between the MAC_{BrC} at 405 nm and the equivalent atmospheric aging time for each SSA classification. Individual burns are shown as gray lines, and the average for each SSA class as the colored line.



105 **Figure S11.** Relationship between the AAE_{BrC} for the 405-532 nm pair and the equivalent
 atmospheric aging time for each SSA classification. Individual burns are shown as gray lines,
 and the average for each SSA class as the colored line. Top row, left-to-right: class 1-3. Bottom
 110 row, left-to-right: class 4-6.

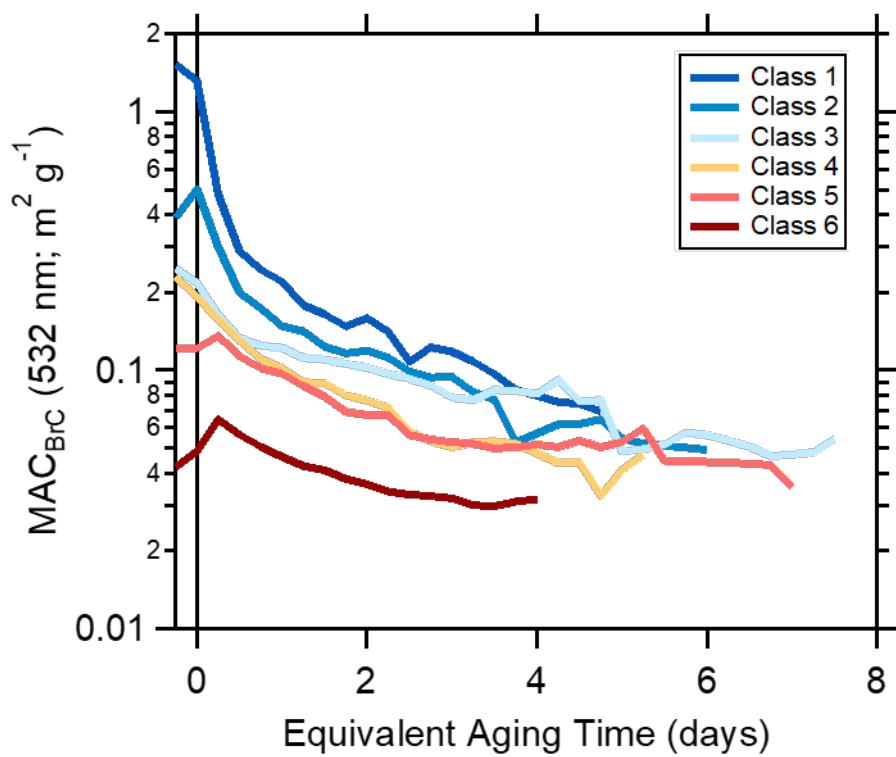


Figure S12. Influence of photochemical aging on MAC_{BrC} at 532 nm. The equivalent aging time assumes $[OH] = 1.5 \times 10^6$ molecules/cm³. The averages for each SSA classification are shown.

115

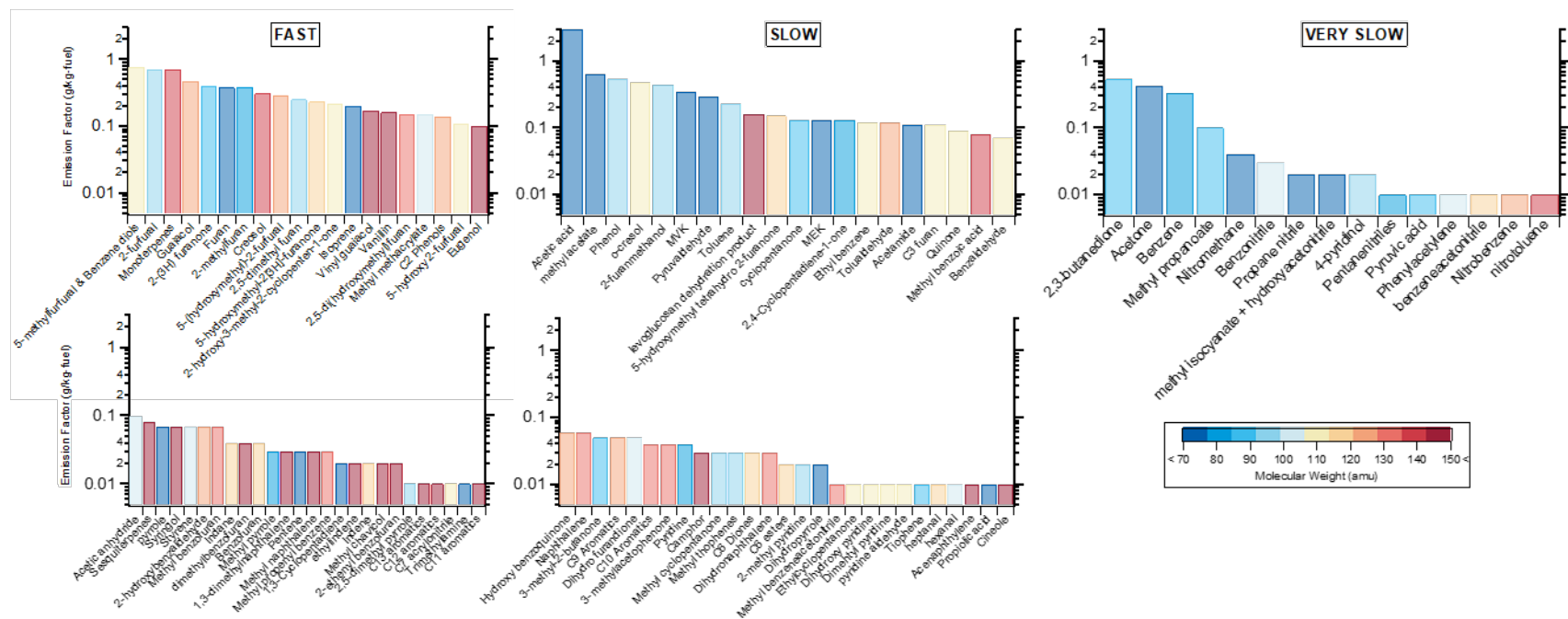
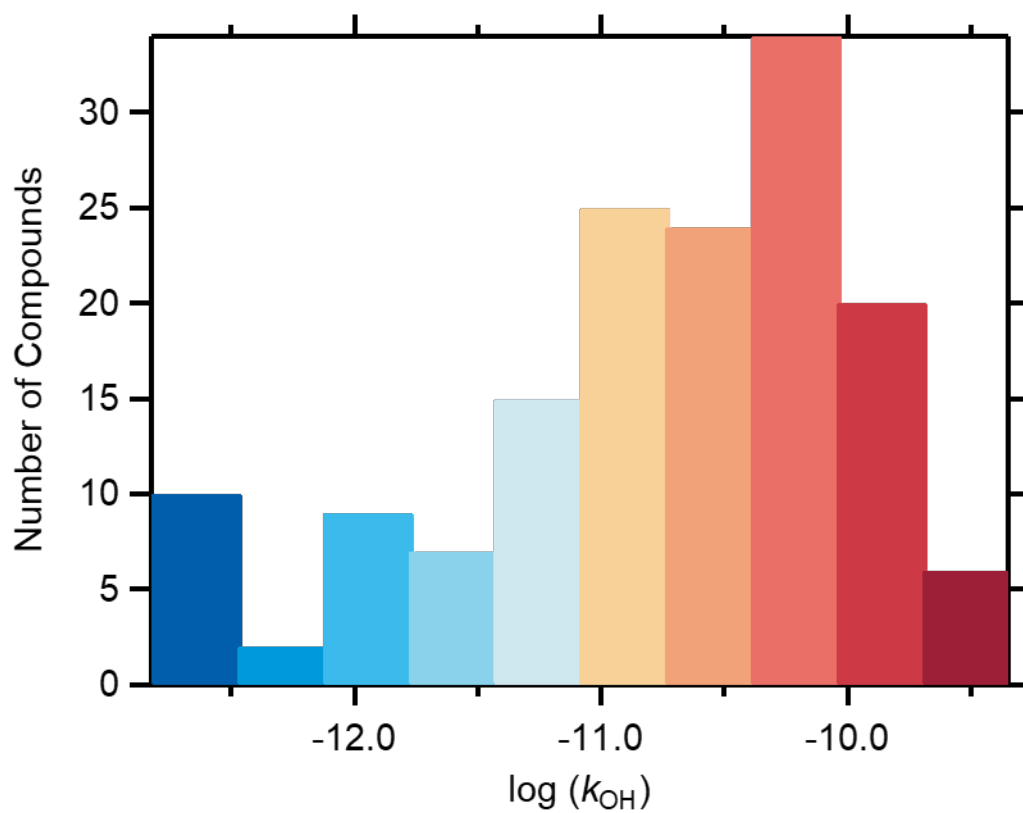
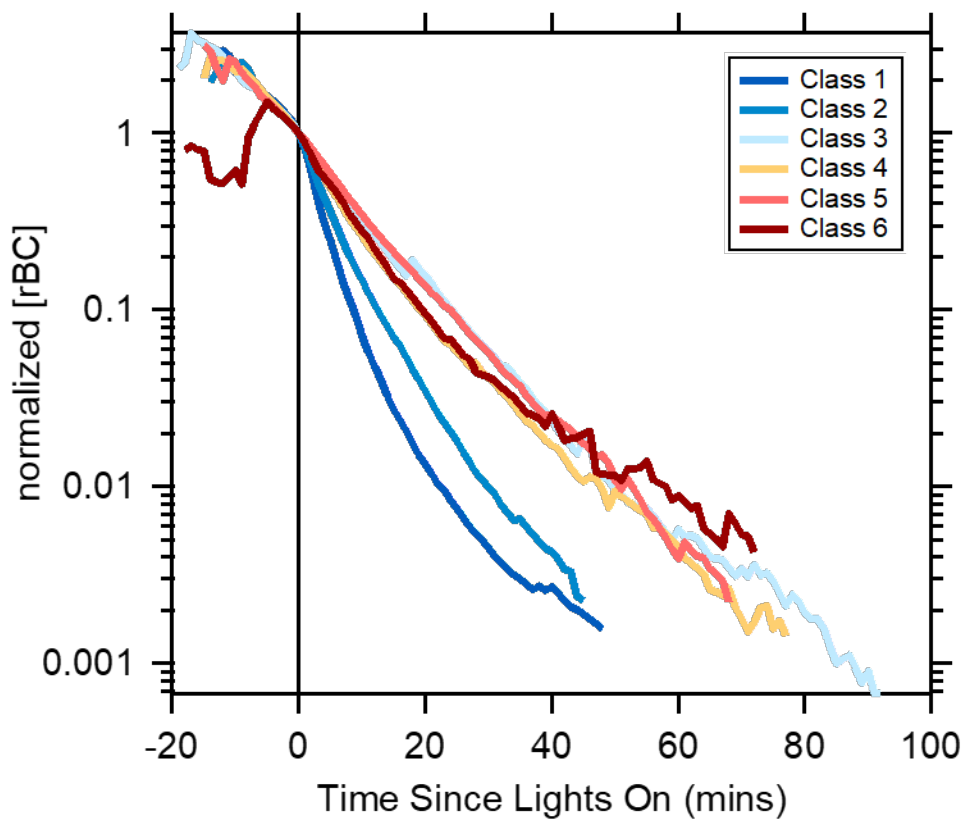


Figure S13. NMOG having MW > 50 amu, grouped into fast reacting, slow reacting and very slow reacting species. For each group, the NMOG are shown ordered according to the overall average emission factors, and are colored by their MW. Data are from Koss et al. (2018).

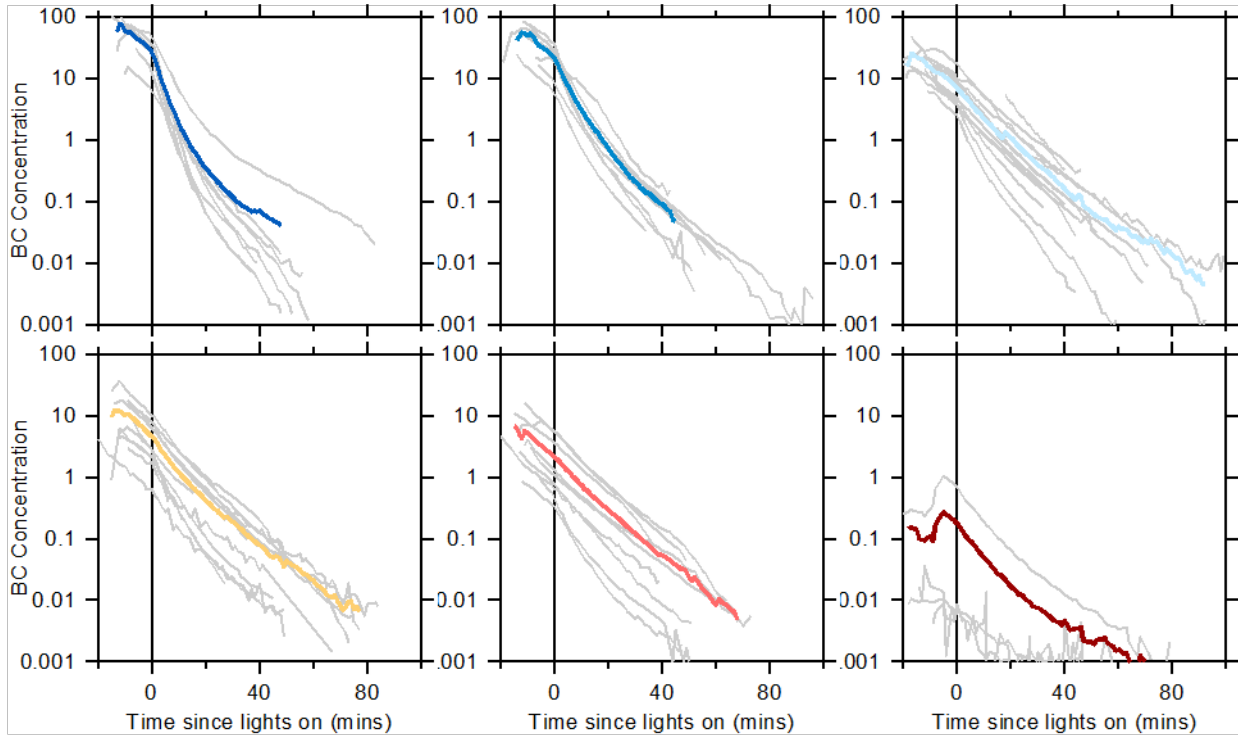


125 **Figure S14.** Histogram of rate coefficients for the NMOG having MW > 50 amu, as measured by Koss et al. (2018).

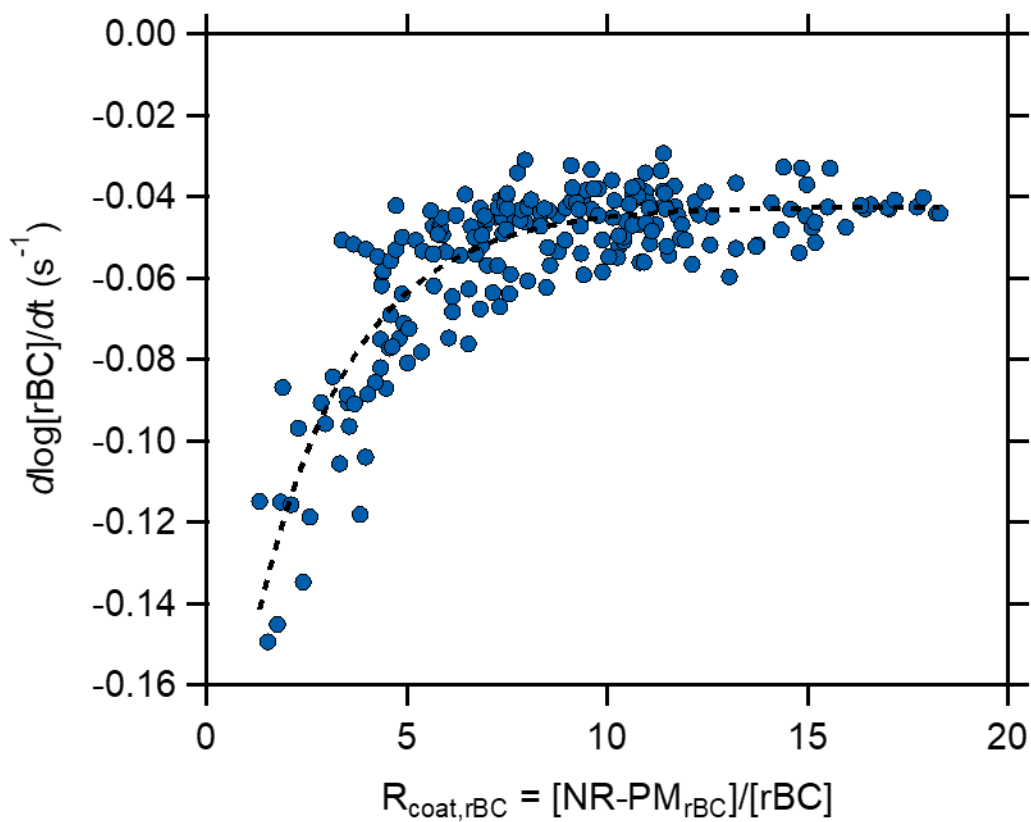


130

Figure S15. Normalized rBC concentration as a function of experiment time, averaged for each SSA classification. Results for each experiment are shown in **Figure S16**.



135 **Figure S16.** Normalized rBC concentration as a function of experiment time, with individual experiments shown as gray lines and the averages for each SSA classification as colored lines.



140 **Figure S17.** Observed loss rate of refractory BC as a function of the coating-to-core mass ratio. The data are fit using an exponential function, with $-\text{dlog}[r\text{BC}]/\text{dt} = -0.0424 - 0.172 \exp(-0.419 R_{\text{coat},r\text{BC}})$.

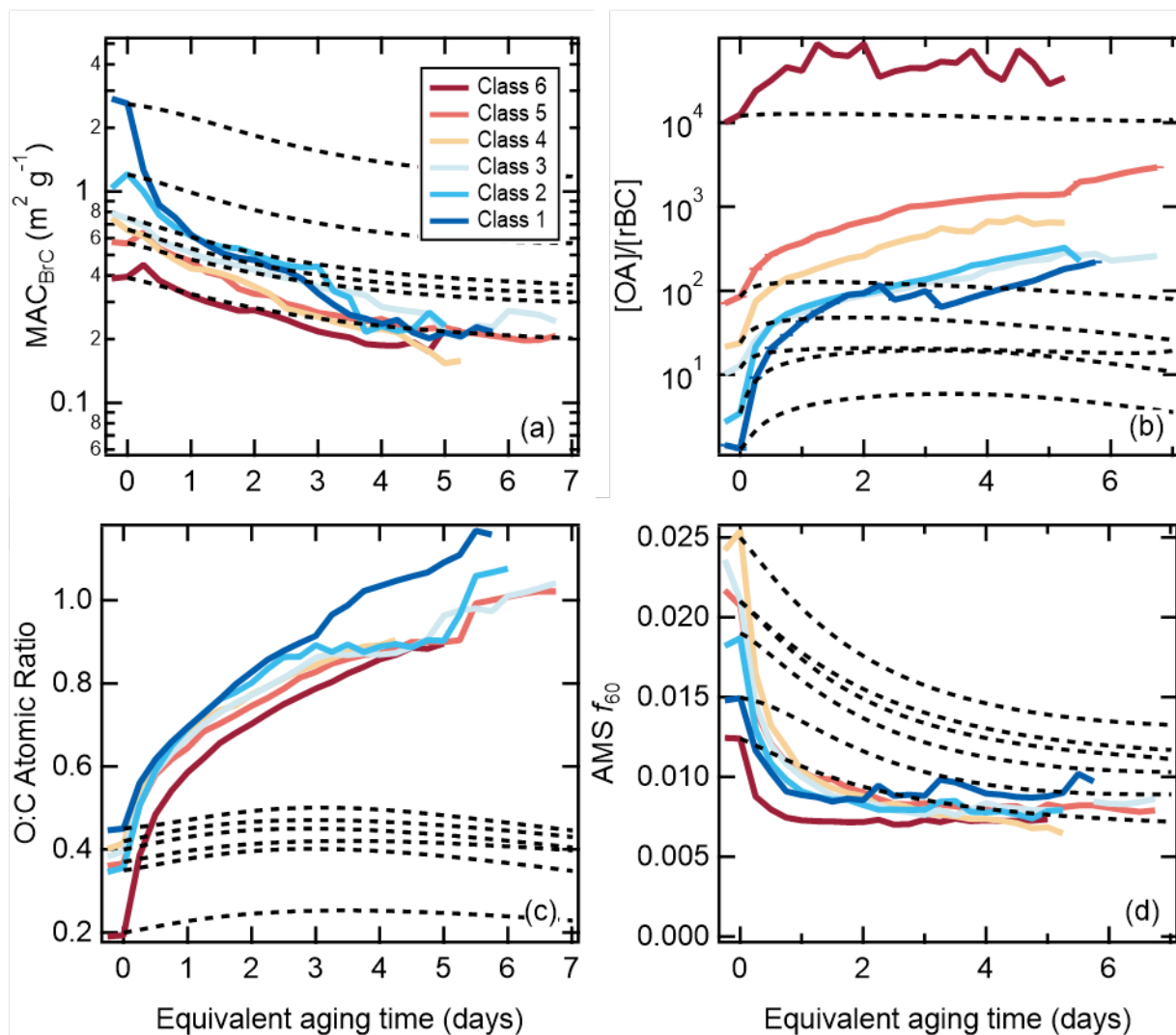
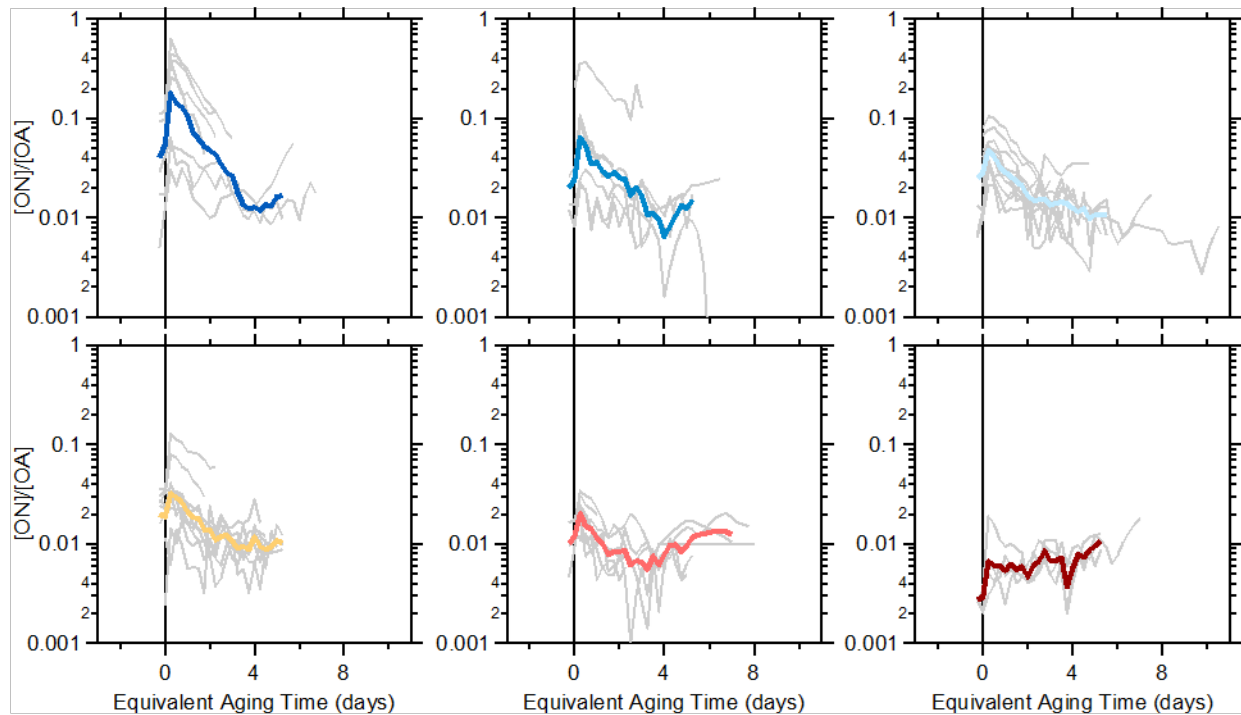


Figure S18. Comparison between observations (solid lines) and model results when only heterogeneous oxidation is included, i.e. no SOA (dashed lines). Results shown for values of the (a) MAC_{BrC} , (b) the $[OA]/[rBC]$ ratio, (c) the O:C atomic ratio, and (d) the $AMS f_{60}$ versus equivalent photochemical aging time (assuming $[OH] = 1.5 \times 10^6$ molecules cm^{-3}), with results shown for each SSA class. The increase in the modeled $[OA]/[rBC]$, despite there being no SOA formation in this model formulation, results from faster loss of OA that is internally mixed with rBC compared with the OA that is externally mixed.

155



160

Figure S19. Dependence of the organic nitrate-to-total OA ratio on equivalent aging time for the different SSA classes. Individual burns are shown as gray lines, and the average for each SSA class as the colored line. Top row, left-to-right: class 1-3. Bottom row, left-to-right: class 4-6.

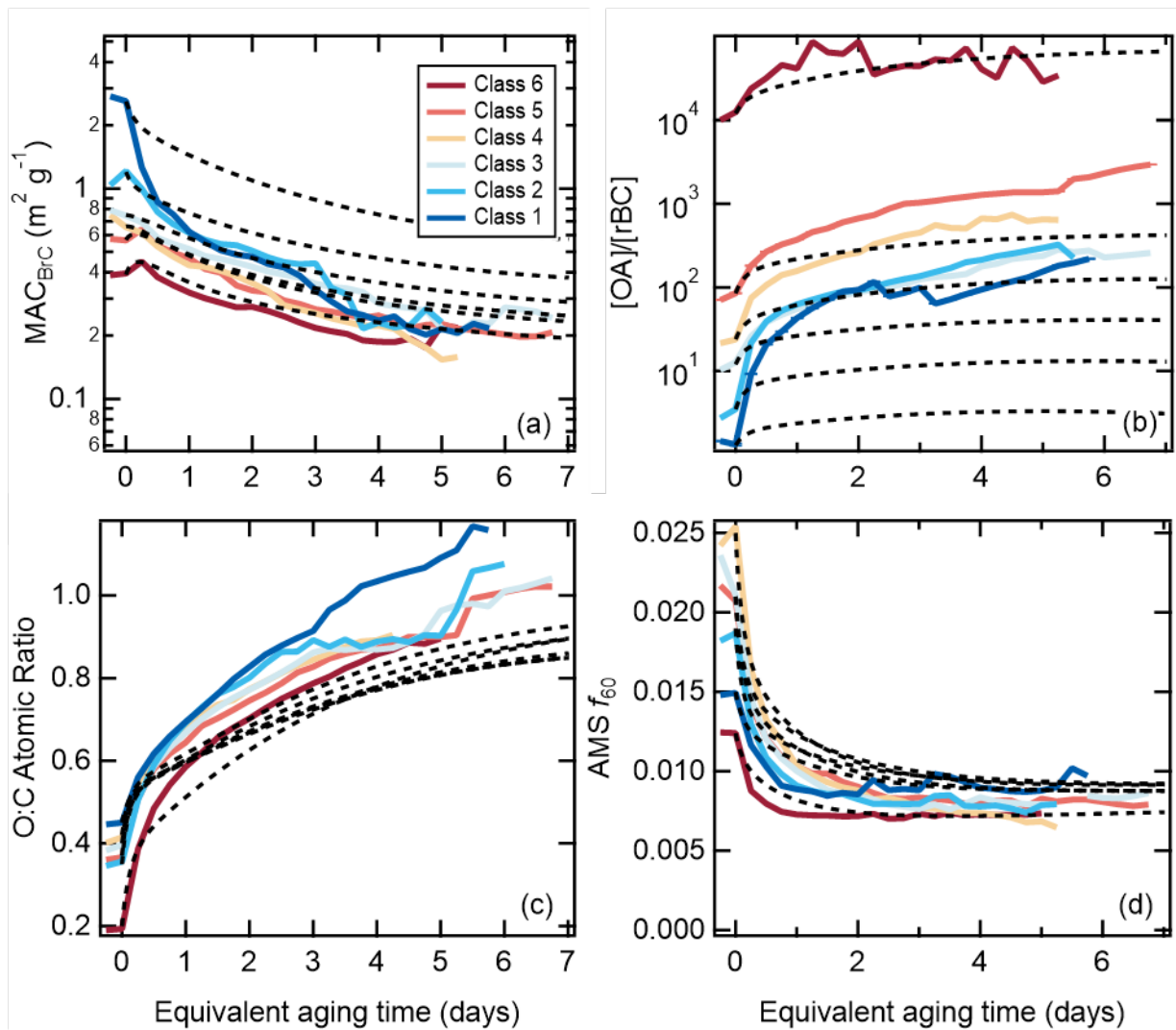


Figure S20. Same as **Figure 3**, but where dilution is turned off entirely for both gases and particles. This corresponds to an “atmospheric” simulation.

3 Supplemental Tables

Table S1. Fuel types used.

Fuel Types*	
bear grass	lodgepole pine, mixed
ceanothus	lodgepole pine, canopy
chaparral (chamise), canopy	lodgepole pine, litter
chaparral (manzanita), canopy	Peat, Kalimantan
Douglas fir, mixed	ponderosa pine, mixed
Douglas fir, canopy	ponderosa pine, canopy
Douglas fir, litter	ponderosa pine, litter
Douglas fir, rotten log	ponderosa pine, rotten log
Engelmann spruce, mixed	rice straw
Engelmann spruce, canopy	sagebrush
Engelmann spruce, duff	subalpine fir, mixed
Engelmann spruce, Fish Lake, canopy	subalpine fir, canopy
Excelsior	subalpine fir, duff
Excelsior (poplar)	subalpine fir, litter
jeffrey pine, duff	subalpine fir
juniper, canopy	untreated lumber
loblolly pine, litter	yak dung

*Further details on each fuel type, including the particular mix for mixed-type burns, elemental composition, and moisture content are available on the NOAA FIREX project website at

Table S2. Instruments sampling from the mini chamber.

Instrument	Property Measured
<i>Particles</i>	
UCD CRD-PAS	Light absorption and dry/humidified light extinction at 405 nm and 532 nm
PASS-3	Light absorption and scattering at 781 nm
CAPS-SSA	Light extinction and scattering at 630 nm
HR-ToF-AMS	Bulk particle non-refractory composition and concentration for PM ₁
SP-AMS	rBC-containing particle composition and concentration for PM ₁
SP2	rBC concentrations and size distributions
SEMS	Mobility size distributions (10-1200 nm)
<i>Gases</i>	
Ozone monitor	O ₃ concentrations
PTR-ToF-MS	Select non-methane organic gases
I-CIMS	Select non-methane organic gases (not used here)
CO ₂	CO ₂ concentrations
RH probe	Relative humidity

180

Table S3. Fuels by particle Class.

Class	Fuel	SSA range	Log([OA]/[BC]) range
Class 1	Chaparral, canopy, litter (pine), building materials, excelsior	0.23-0.43	-0.52 – 0.38
Class 2	Manzanita, Sage, litter (fir)	0.43-0.60	0.18 – 0.61
Class 3	Pine, fir, litter, canopy, juniper	0.60-0.74	0.82 – 1.3
Class 4	Pine, fir, canopy, rotten log, ceonothos	0.74-0.87	0.92 – 1.74
Class 5	Canopy (pine), rice, bear grass, duff	0.87-0.93	1.49 – 2.16
Class 6	Rotten log, duff, peat, dung	0.93-1.00	2.63 – 2.02

Table S4. Summary of conditions for literature brown carbon aging experiments.

Reference	Aging method/notes	Fuel type/burning notes
Martinsson et al. (2015)	Aging of smoke in oxidation flow reactor (potential aerosol mass reactor); 370 nm; $t_{OH} = 8.3$ days; Observed notable decrease in absorptivity after aging	Birch; Combustion in a natural-draft conventional wood stove; likely class 1 to class 3 particles
Saleh et al. (2013)	Photochemical aging of smoke in 7 m ³ chamber for $t_{OH} \sim$ a few hours; aging of pine likely > oak; Report SOA absorptivity < POA absorptivity	Pocosin pine and oak; combustion at Missoula fire lab; likely class 1 particles
Zhong and Jang (2014)	Photochemical aging of smoke in a 104 m ³ outdoor chamber using natural sunlight; $t_{OH} =$ a few hours; continual characterization; Observed initial increase in absorptivity to 2 h followed by gradual decline	Hickory hardwood; Smoldering combustion; likely class 5
Kumar et al. (2018)	Photochemical aging of smoke in an 8 m ³ chamber; t_{OH} up to a day; Interpolate their observations to 405 nm; Observed increase in AAE with aging	Beechwood; combustion in a residential wood stove; likely class 1
Sumlin et al. (2017)	Rapid heterogeneous OH aging in an oxidation flow reactor (potential aerosol mass reactor); $t_{OH} = 1, 3.5, 4.5$ days; Observed non-monotonic change in absorptivity	Alaskan peak; smoldering; likely class 6
Wong et al. (2017)	Photolytic aging (300-400 nm) of water-soluble and water-insoluble (methanol) extracts in a photoreactor; up to 130 h; photolysis of solutions; Observed continuous decrease in absorptivity	Cherry hardwood; Controlled pyrolysis; likely class 6, although measurements of suspended particles not available
Lee et al. (2014)	Photolytic aging (275-390 nm) of aqueous extracts; photolysis of solutions	SOA produced from naphthalene + OH
Fleming et al. (2020)	Photolytic aging (300-400 nm) of particles on filters; absorption by individual chromophores or total particles measured; wide range of equivalent lifetimes with respect to photolysis observed for different chromophores	Variety of fuels from FIREX, comprising different species and ecosystem components; range of particle classes likely
Browne et al. (2019)	Rapid heterogeneous OH aging in a flowtube; equivalent t_{OH} up to 1.2 h; Observed continuous decline in BrC absorptivity	Smoldering combustion of ponderosa pine needles; negligible BC, likely class 6
Cappa et al. (2019)	Ambient observations in Fresno, CA, where the properties of wood smoke OA were estimated from multi-linear regression of the observed absorption and the time-varying concentrations of individual factors from PMF analysis of the organic aerosol	Smoke likely derived from wood combustion for home heating in fireplaces and stoves; based on MAC_{BrC} and AAE , likely similar to class 2

185 4 Supplemental References

- Browne, E. C., Zhang, X., Franklin, J. P., Ridley, K. J., Kirchstetter, T. W., Wilson, K. R., Cappa, C. D., and Kroll, J. H.: Effect of heterogeneous oxidative aging on light absorption by biomass burning organic aerosol, *Aerosol Science and Technology*, 53, 663-674, <https://doi.org/10.1080/02786826.2019.1599321>, 2019.
- 190 Cappa, C. D., Zhang, X., Russell, L. M., Collier, S., Lee, A. K. Y., Chen, C.-L., Betha, R., Chen, S., Liu, J., Price, D. J., Sanchez, K. J., McMeeking, G., Williams, L. R., Onasch, T. B., Worsnop, D. R., Abbatt, J., and Zhang, Q.: Light absorption by ambient black and brown carbon and its dependence on black carbon coating state for two California, USA cities in winter and summer, *Journal of Geophysical Research-Atmospheres*, 124, 1,550-551,577, <https://doi.org/10.1029/2018JD029501>, 2019.
- 195 Fleming, L. T., Lin, P., Roberts, J. M., Selimovic, V., Yokelson, R., Laskin, J., Laskin, A., and Nizkorodov, S. A.: Molecular composition and photochemical lifetimes of brown carbon chromophores in biomass burning organic aerosol, *Atmos. Chem. Phys.*, 20, 1105-1129, <https://doi.org/10.5194/acp-20-1105-2020>, 2020.
- 200 Kumar, N. K., Corbin, J. C., Bruns, E. A., Massabó, D., Slowik, J. G., Drinovec, L., Močnik, G., Prati, P., Vlachou, A., Baltensperger, U., Gysel, M., El-Haddad, I., and Prévôt, A. S. H.: Production of particulate brown carbon during atmospheric aging of wood-burning emissions, *Atmos. Chem. Phys.*, 2018, 17,843-817,861, <https://doi.org/10.5194/acp-18-17843-2018>, 2018.
- 205 Lee, H. J., Aiona, P. K., Laskin, A., Laskin, J., and Nizkorodov, S. A.: Effect of Solar Radiation on the Optical Properties and Molecular Composition of Laboratory Proxies of Atmospheric Brown Carbon, *Environmental Science & Technology*, 48, 10217-10226, <https://doi.org/10.1021/es502515r>, 2014.
- Martinsson, J., Eriksson, A. C., Nielsen, I. E., Malmberg, V. B., Ahlberg, E., Andersen, C., Lindgren, R., Nyström, R., Nordin, E. Z., Brune, W. H., Svenningsson, B., Swietlicki, E., Boman, C., and Pagels, J. H.: Impacts of Combustion Conditions and Photochemical Processing on the Light Absorption of Biomass Combustion Aerosol, *Environmental Science & Technology*, 49, 14663-14671, <https://doi.org/10.1021/acs.est.5b03205>, 2015.
- 210 Saleh, R., Hennigan, C. J., McMeeking, G. R., Chuang, W. K., Robinson, E. S., Coe, H., Donahue, N. M., and Robinson, A. L.: Absorptivity of brown carbon in fresh and photochemically aged biomass-burning emissions, *Atmospheric Chemistry and Physics*, 13, 7683-7693, <https://doi.org/10.5194/acp-13-7683-2013>, 2013.
- 215 Sumlin, B. J., Pandey, A., Walker, M. J., Pattison, R. S., Williams, B. J., and Chakrabarty, R. K.: Atmospheric Photooxidation Diminishes Light Absorption by Primary Brown Carbon Aerosol from Biomass Burning, *Environmental Science & Technology Letters*, 4, 540-545, <https://doi.org/10.1021/acs.estlett.7b00393>, 2017.
- 220 Wong, J. P. S., Nenes, A., and Weber, R. J.: Changes in Light Absorptivity of Molecular Weight Separated Brown Carbon Due to Photolytic Aging, *Environmental Science & Technology*, 51, 8414-8421, <https://doi.org/10.1021/acs.est.7b01739>, 2017.
- 225 Zhong, M., and Jang, M.: Dynamic light absorption of biomass-burning organic carbon photochemically aged under natural sunlight, *Atmospheric Chemistry and Physics*, 14, 1517-1525, <https://doi.org/10.5194/acp-14-1517-2014>, 2014.